Journal of Materials Science: Materials in Electronics
https://doi.org/10.1007/s10854-019-01079-5

Ultra-low temperature co-fired CaV_2O_6-glass composite ceramic substrate for microelectronics

Arun Sasidharanpillai[1,2] · Sebastian Mailadil Thomas[1] · Younki Lee[2] · Hyo Tae Kim[1]

Received: 2 February 2019 / Accepted: 5 March 2019

Abstract
Bivalent calcium metavanadate (CaV_2O_6) ceramic-glass composite substrates were fabricated using non-aqueous environmental friendly tape casting formulation. 3 wt% of commercial glass was added to the calcined powder of CaV_2O_6 to achieve a sintering temperature of 650 °C which enables ultra-low temperature co-firing with aluminum electrode. An environmentally benign binder/solvent (Polypropylene carbonate/dimethyl carbonate) system was adopted to prepare the well dispersed slurry for tape casting. The crystal structure and co-fireability of the sintered substrate with Al was verified by X-ray diffraction technique. Thermal, dielectric and morphological analysis of the multilayer were analyzed. The room temperature thermal conductivity of CaV_2O_6-glass composite sintered at 650 °C is about 2.8 W/m K. Sintered ceramics shows a relatively high linear coefficient of thermal expansion (CTE) of 11.46 ppm/°C, which is favorable for co-firing with high CTE metallic materials. Microwave dielectric properties of CaV_2O_6-glass composite multilayer fired at 650 °C are $\varepsilon_r = 10.6$ and $\tan\delta = 3.19 \times 10^{-4}$ at 15 GHz.

1 Introduction

Low Temperature Co-fired Ceramic (LTCC) is an established multilayer circuit fabrication technology widely used in electronic, military and automotive industry where multi-functionality, miniaturization and reliability are major demands [1–3]. Its stable physical and electronic properties over wide temperature range and environments help its application in military and automotive industry. High process yield, high component density, ease of manufacture and possibility of co-firing with conductive, dielectric or resistive thick film inter-layers are the advantages from which microelectronic industry is benefitted. One of the leading advantages of LTCC technology is that highly conducting metals such as Ag, Cu and Au can be co-fired with it. Conventional LTCC systems are achieved through liquid phase sintering of high melting oxide ceramic by adding finite amount of low melting glass with it [2]. However, addition of glass leads to degradation of mechanical strength and microwave dielectric properties of the fabricated substrate.

In order to reduce the cost of multilayer devices, nowa-days, researchers are more focused on developing new low loss materials possessing ultra-low sintering temperature (ULTCC systems), (< 700 °C) for co-firing with low cost and highly conducting metal, aluminum electrodes [4]. Most of the candidates belongs to ULTCCs are compositions containing TeO_2, MoO_3, WO_3, Bi_2O_3 or V_2O_5 [5–9]. Recently, extensive researches have been made in vanadate based ceramic systems, since they possess ultra-low sintering temperature with promising dielectric properties in the microwave frequency range. There are many reports on V_2O_5 based ULTCC materials such as $LiMoVO_6$, $LiWVO_6$, $Ba_{16}V_{18}O_{61}$, BaV_2O_6, $Ba_3V_4O_{13}$, and CaV_2O_6 [10–14]. Among the vanadates CaV_2O_6 is reported to have the highest quality factor, $Q \times f = 123{,}000$ GHz at 10.2 GHz with a dielectric constant, $\varepsilon_r = 10.2$ and a negative temperature co-efficient of resonant frequency, $\tau_f = -60$ ppm/°C [13].

Tape casting is a well-established fabrication process for large area ceramic substrate, multilayer ceramic capacitors, solid oxide fuel cells etc. Aqueous and non-aqueous based slurry formulations are practiced for different ceramic tape casting systems. Organic slurry formulations are frequently used, where high volatility, good wetting properties and high quality of green tapes are the primary requirements, whereas

✉ Hyo Tae Kim
hytek@kicet.re.kr

[1] Korea Institute of Ceramic Engineering and Technology, Jinju 52851, Republic of Korea

[2] Department of Materials Engineering and Convergence Technology, RIGET, Gyeongsang National University, Jinju 52828, Republic of Korea

Published online: 13 March 2019

aqueous based formulations are applied on consideration of the environmental and health hazards [15, 16]. Green tapes fabricated out of organic slurries are mostly free of cracks due to the weak capillary force during drying compared to its counterpart [17]. Water based slurry systems face challenges such as slower drying rates, high dielectric constant of water, warping during sintering etc. Recently, reports are available for non-aqueous environmental friendly tape casting slurry formulation, which can combine advantages of both the aqueous and organic system. Carbonate based environmental friendly binder-solvent compositions are successfully applied for ultra-low firing tape casting slurries [18, 19].

There are only a couple of reports available for tape casting of ultra-low temperature co-fired ceramic materials and most of them are prepared using organic solvents and binders [20, 21]. In this study, we have investigated structural, thermal and dielectric properties of ultra-low temperature cofireable CaV_2O_6-glass composite tape synthesized through a newly suggested eco-friendly tape casting process.

2 Experimental

2.1 Synthesis of CVO ceramic

CaV_2O_6 (CVO) was synthesized by conventional solid state ceramic route by using stoichiometric amount of high purity chemicals of $CaCO_3$ and V_2O_5. The precursors were mixed and ball milled in ethanol medium for 24 h using yttria stabilized zirconia balls. The dried powder was calcined at 650 °C for 4 h for getting phase pure monoclinic phase of CaV_2O_6. To reduce the particle size as required for tape casting, the calcined powder was ball milled using high energy planetary ball mill for 5 h. The size reduced powder was pressed into cylindrical pucks at a pressure of 200 MPa and sintered at a temperature of 740 °C for 4 h. For reducing the sintering temperature, the CVO was mixed with 3 wt% of commercial glass powder (Glass code: 29607, Ceradyne, Inc., 3M) and the dried powder was sintered at 650 °C for a holding time of 4 h. The chemical compatibility of the glass added CVO was checked by mixing it with 20 wt% of aluminum powder (High Purity Chemicals, Kojundo Korea Co. Ltd.) and sintered at 650 °C for 4 h. The structural confirmation of the sintered ceramics was conducted by X-ray diffraction spectroscopy using Cu K-α radiation (RIGAKU RINT 2000). The density of the sintered CVO and CVO-glass composite ceramic was measured using Archimedes' method. The linear co-efficient of thermal expansion of sintered ceramics was analyzed by thermo mechanical analyzer (TMA Q 400, TA Instruments) and the thermal conductivity was measured using laser flash thermal analysis (LFA 427, NETZSCH).

2.2 Synthesis of CVO-glass composite tape

An environmental friendly slurry system was used for tape casting, in which dimethyl carbonate and polypropylene carbonate (QPAC 40, Empower Materials, Inc., USA) was used as the solvent and binder respectively. Proper dispersion for the slurry was achieved by using Nopcosperse 92 (San Nopco Ltd. Tokyo) as dispersant. The slurry preparation was done in two stages, in the first stage, powder was dispersed with dispersant and solvent and is ball milled for 24 h. Suitable additives such as binder (QPAC 40) and plasticizers (Dibutyl Phthalate, Polyethylene Glycol) were added to the dispersed slurry in the second stage for providing strength and flexibility for the green tape and is again kept for mixing for 24 h. The viscosity of the final tape casting slurry was carried out by Rheometer (Digital Viscometer, BROOKFIELD DV-II Pro, USA). Homogeneous and uniform green tape of CVO-glass composite was casted using tape casting machine (TCA-2000, Techgen, Korea). The thermo-gravimetric analysis (TGA) of the green tape was done by simultaneous DTA-TG apparatus (DTG-60H, Shimadzu, Kyoto, Japan). The ultimate tensile strength (UTS) of the optimized tape was tested using universal testing machine (Instron 5544, North America). For further characterization, the dried tape was cut into square pieces and thermo-laminated together at a temperature and pressure of 60 °C and 65 MPa respectively using a thermo-laminator. The laminated tape was sintered at a temperature of 650 °C for a holding time of 4 h. The surface morphology of the green, thermo-laminated and sintered tapes of CVO-glass composite were observed and recorded using a field emission scanning electron microscopy (JEOL/JSM-6700F, Oxford). The surface roughness of the green and sintered tapes of CVO-glass composite was characterized by atomic force microscopy (AFM) (WITEC, Focus Innovations, Germany) operating in the tapping mode. The dielectric properties of the sintered tape in the low frequency region were analyzed by precision impedance analyzer (4294A, Agilent Technologies, Santa Clara, CA). The microwave dielectric properties of the sintered laminates at 15 GHz was analyzed in a split post dielectric resonator (QWED, Warsaw, Poland) with the aid of a network analyzer (8720ES, Agilent Technologies, Santa Clara, CA).

3 Results and discussion

3.1 Structural characterization

Bivalent metal metavanadate crystallizes into four main type of structure in which CaV_2O_6 have been found to

crystallize in the monoclinic Brannerite (B2-type) with space group C2/m dominated by the presence of ladder-type $\{V_2O_6\}$ chains made of edge-shared VO_5 square pyramids (Fig. 1a) [22]. The system can be described as being consists of distorted VO_6 octahedra, which share opposite corners and forms chains running parallel to the b axis of the unit cell [23]. Perez et al. and Bouloux et al. conducted detailed structural investigation of CaV_2O_6 and reported atomic co-ordinates, cell parameters and structural model for this compound [24, 25]. XRD pattern of CVO sintered at 740 °C is shown in Fig. 1b, which is exactly matching with monoclinic structure suggested by Perez et al. All the observed peaks are indexed using Powder Diffraction File no. 73-0971 [Joint Committee on Powder Diffraction Standards, (1970)]. XRD pattern of CVO-glass composite co-fired with Aluminum at 650 °C is shown in Fig. 1b. There is no reactivity is observed between Al metal and ceramic-glass system at this temperature and the additional peaks (represented as *) are from Al, based on Powder Diffraction File no. 85-1327 [Joint Committee on Powder Diffraction Standards, (1953)].

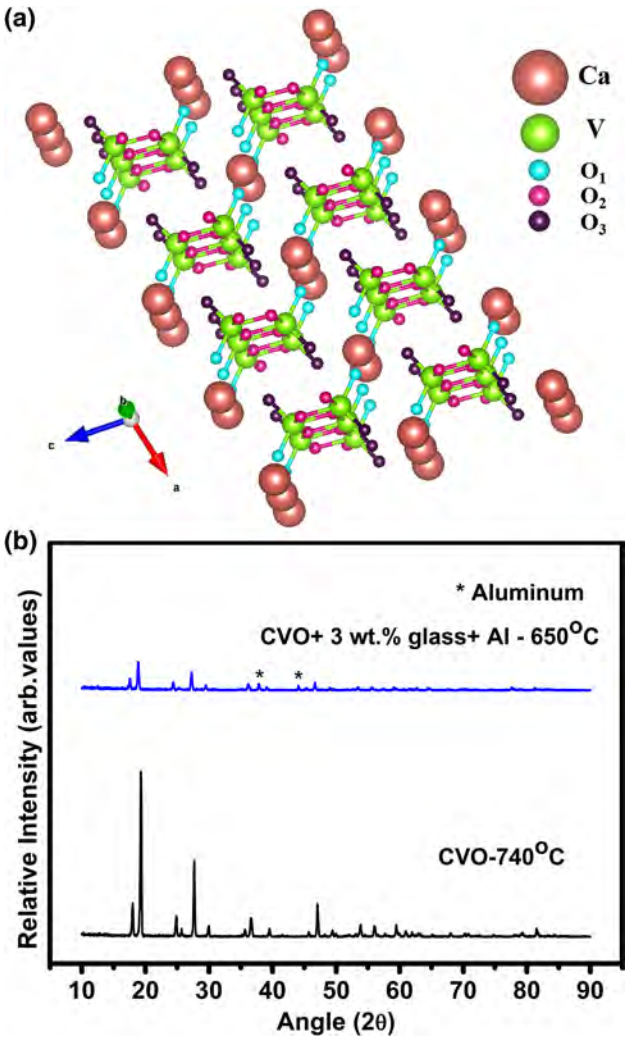

Fig. 1 **a** Crystal structure of CVO and **b** XRD pattern of CVO

3.2 Rheological properties

The strength and thickness uniformity of the casted tape depends on many parameters such as the viscosity of the slurry, casting speed and geometrical dimension of the casting head [26]. Chou et al. first theoretically studied the behavior of ceramic slurry possessing Newtonian character by employing fluid flow model. In fluid flow model, the flow of the slurry within the channel was modeled as a linear combination of a drag flow and a pressure [27]. In reality, tape casting slurries are complex multicomponent suspension, which do not follow a Newtonian character. Tok et al. proposed a new model by considering all the drawback of the previous model by assuming the slurry as a non- Newtonian pseudoplastic fluid following the Ostwald de Waele power law constitutive model. As shown in Fig. 2, the relationship between shear stress and shear rate is non-linear, which is in well agreement with the model suggested by Tok et al. Hence the slurry is following a non-Newtonian behavior with a pseudoplastic nature [28]. Viscosity is largely influenced by the solid content as well as the amount of binder in the slips. Both the degree of pseudo-plasticity and viscosity increases with increase in solid content and binder ratio. The viscosity of the slurry decreases with increase in shear rate as shown in Fig. 2, is a necessary requirement for a tape casting slurry. This shear thinning behavior is due to the gradual breaking of the bonding network formed while the slurry was in rest [18]. Table 1 shows the composition of the final tape casting slurry, with optimized amount of dispersant, binder and plasticizer. The casted green tape shows an UTS of 0.30 MPa [29, 30].

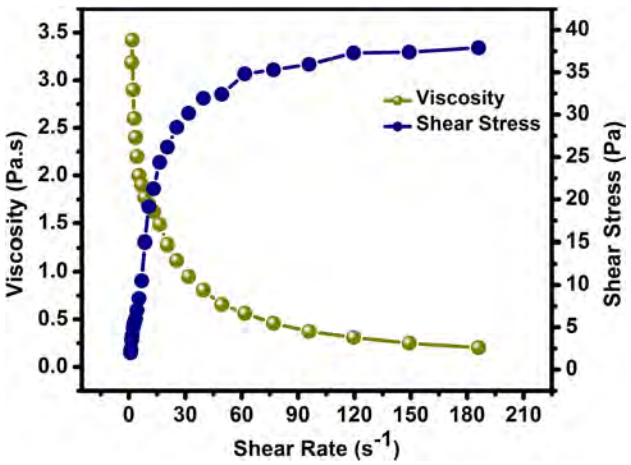

Fig. 2 Variation of viscosity and shear stress with shear rate for final tape casting slurry of CVO-glass composite

Table 1 Composition for the final tape casting slurry

Component	Composition (wt%)	Function
First stage		
CaV_2O_6 + 3 wt% glass	43.7	Filler
Nopco 092	0.40	Dispersant
Dimethyl carbonate	49.2	Solvent
Second stage		
Polypropylene carbonate	5.9	Binder
Dibutyl phthalate	0.57	Plasticiser (type I)
Poly ethylene glycol-300	0.20	Plasticiser (type II)

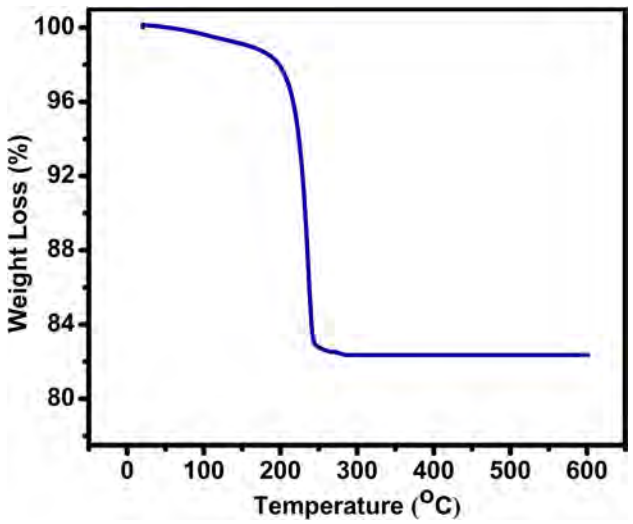

Fig. 3 TGA of CVO-glass composite tape

3.3 TGA

Poly propylene carbonate (PPC), an environmental friendly binder, possess very low decomposition temperature (< 300 °C) compared to conventional organic binders such as polyvinyl butyral (PVB), polyvinyl alcohol (PVA), methyl cellulose, starch etc. These characteristics are very helpful in the development of defect free substrates for the ULTCC technology where the firing temperature is below 660 °C [18, 31]. As well as the clean burnout property of PPC through an unzipping mechanism even in an inert atmosphere helps its application for ceramic materials in oxidizing environment. Yan et al. conducted detailed investigation on thermal decomposition mechanism of PPC in both air and nitrogen atmosphere using TGA. PPC binder decomposes by combustion enhanced depolymerisation mechanism into CO_2 and water without leaving a residue. The initial and final decomposition temperature of PPC itself in air is 255 °C and 300 °C respectively [32–35]. From the TGA plot (Fig. 3), it is clear that a two-step weight loss is occurred for the CVO-glass composite tape, in which a rapid initial decomposition between 190 and 245 °C, followed by a slow rate which stops at 290 °C. As explained by Masia et al. the oxide ceramic has a catalytic effect on the decomposition of polymer binder and the reduction in decomposition temperature of PPC from the reported value is expected to be due to the catalytic effect of CVO ceramic powder. In Fig. 3, the difference between the initial and final decomposition temperature of the composite is approximately 100 °C, which is higher than the difference in pure PPC (~ 45 °C) [36]. Hence it is concluded that presence of CVO-glass oxide ceramic not only provided catalytic effect but also slowed down the decomposition rate of PPC in the green tape. Due to the complete early stage binder burnout, the weight was observed to be stable after 290 °C and is crucial for defect free final product [18].

3.4 Morphological characterization

A highly porous microstructure is observed for the green tape (single layer) due to the evaporation of solvent from the surface and is visible in Fig. 4a. Figure 4b shows the cross section of a thermo-laminated stack of eight layers of CVO-glass composite tape. The applied thermo-lamination condition is sufficient to form a green stack without any crack or delamination. Liquid phase sintering is a useful processing technique to control the grain growth during sintering to fabricate mechanically strong ceramic substrate. As shown in Fig. 4c, d, the addition of 3 wt% of glass powder promotes early-stage densification and alleviates the abnormal grain growth. There is hardly any abnormal grain growth observed for CVO-glass composite multilayer sintered at 650 °C.

The surface roughness and the metal-ceramic interface of the printed pattern play a significant role in the dielectric loss of an LTCC substrate. The corrugations on the surface of ceramic tape and metal pattern can manipulate the capacitance, inductance and resistance of the ceramic substrate which is able to increase the loss in these circuits. The uniformity of the printed pattern depends directly on the surface evenness of the green ceramic tape on which the pattern is printed [37]. In addition to that the mobility of the electrons in the printed metallization strongly depends on the roughness of the substrate and the carrier trapping is more prominent on rougher substrates [38, 39]. Figure 5a, b shows the atomic force microscopic images of green and sintered tapes of CVO-glass composite. The green tape has an average roughness of 402 nm and that of tape sintered at 650 °C is 140 nm.

3.5 Dielectric properties

Generally, the extrinsic loss of a dielectric material is affected by many factors such as, porosity, impurities, oxygen

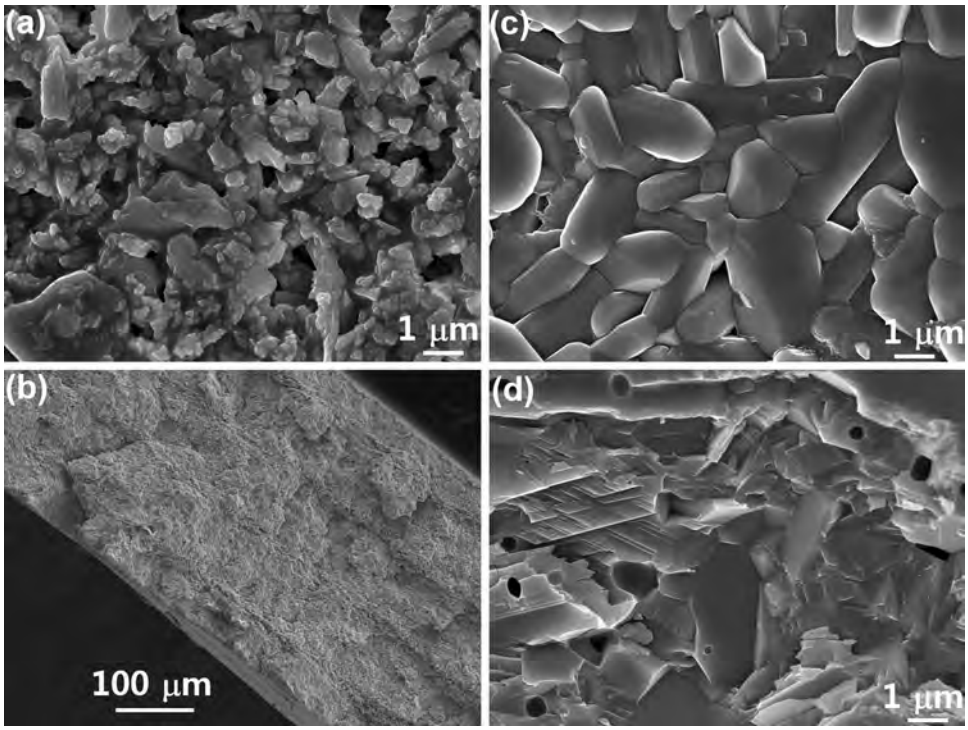

Fig. 4 **a** Surface morphology of green tape (single layer) **b** fractured surface of green laminate **c** surface morphology and **d** fractured surface of CVO-glass composite tape sintered at 650 °C (eight layer)

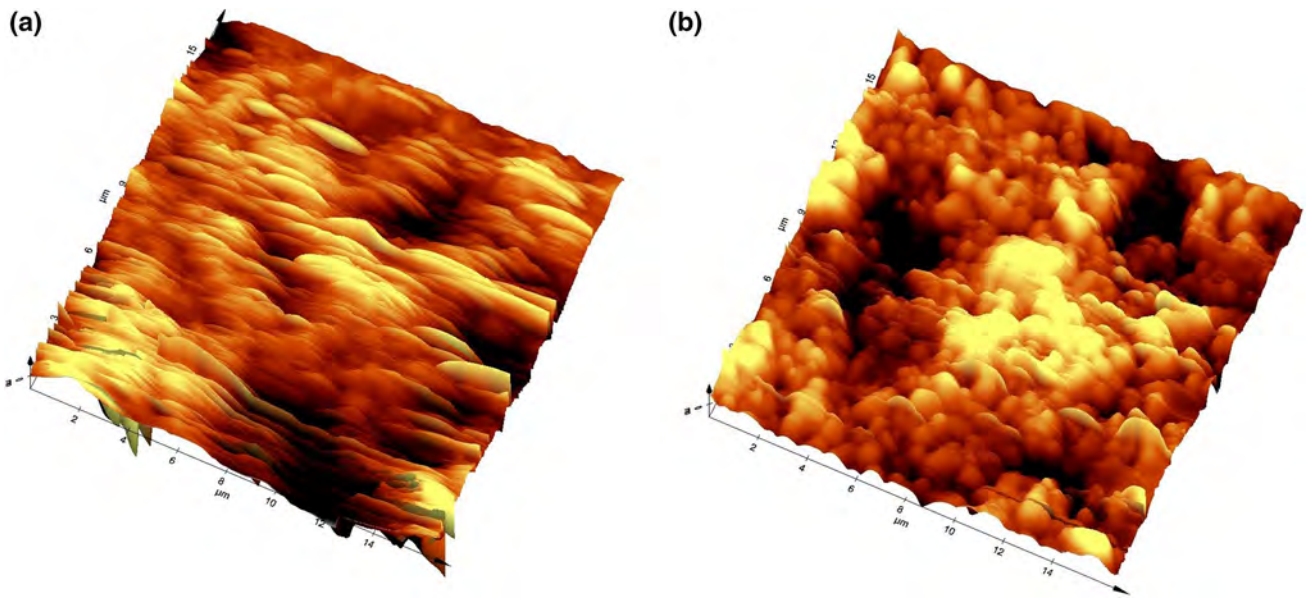

Fig. 5 AFM image of the surface of **a** green tape and **b** sintered tape of CVO-glass composite

vacancies, second phase, grain size, etc. Neelakantan et al. investigated the microwave dielectric properties of ultra-low temperature sintered BaV_2O_6 ceramic (550 °C) and reported dielectric constant of 11.2 and a Q × f of 42,790 GHz [12]. Suresh et al. has reported the dielectric properties of a series of vanadates ULTCC systems, $Ba_{16}V_{18}O_{61}$ ($\varepsilon_r = 9.7$, Q × f = 80,100), $Sr_{16}V_{18}O_{61}$ ($\varepsilon_r = 9.8$, Q × f = 75,600) and $Ca_{16}V_{18}O_{61}$ ($\varepsilon_r = 11.1$, Q × f = 79,100) at ≈ 12 GHz [11]. In the present work CVO tape (ten layer) sintered at 725 °C shows $\varepsilon_r = 11.1$ and $\tan\delta = 1.21 \times 10^{-4}$ at 15 GHz, whereas its glass composite tape (CVO + 3 wt% glass) sintered at 650 °C possess $\varepsilon_r = 10.6$ and $\tan\delta = 3.19 \times 10^{-4}$ at 15 GHz. Table 2 lists the microwave dielectric properties of sintered tapes of CVO and CVO-glass composite at 15 GHz. It is

Table 2 Dielectric properties of CVO and CVO-glass composite tape at 15 GHz

Material	Sintering temperature °C/4 h	Densification (%)	No. of layers	Thickness mm	Microwave dielectric properties at 15 GHz	
					ε_r	tanδ
CVO	725	95	10	0.55	11.1	1.21×10^{-4}
CVO + 3 wt% glass	650	96	8	0.50	10.6	3.19×10^{-4}

obvious that presence of finite amount of glass affects the dielectric properties of the ceramic material [40, 41]. The decrease in the ε_r of CVO-glass composite is due to the presence of low ε_r amorphous phase in it. The glass addition not only decreased ε_r but also increased tanδ of CVO-glass composite tape compared to its pure form [42]. Addition of sintering aids affects the ceramics in different ways by changing density, microstructure, defect structure, and possibly crystal structure. These changes, brought about by the sintering aids, which control the dielectric properties of the materials [43]. The low frequency variation of ε_r and tanδ of CVO and its glass composite ceramic sintered at 740 °C and 650 °C respectively is shown in Fig. 6a, b.

3.6 Thermal conductivity

LTCC materials normally have an intrinsically low thermal conductivity (3–5 W/m K), which limits its applications in high power circuits [44]. Thermal conductivity of commercial LTCC tape ranges from 2 to 4.5 W/m K [45]. LTCC materials possessing higher thermal conductivity greater than 5 W/m K were already reported, but most of them are Al_2O_3 based glass–ceramic systems, in which the presence of large amount of glass deteriorates the dielectric properties [46, 47]. Wang et al. had reported LTCC composition with very high thermal conductivity of 38.9 W/m K by adding Cu fiber with Al_2O_3/glass system. But the presence of conducting material in it limits its use in microelectronic circuits, where low loss is one of the major criterion [48]. Figure 7a, b shows the variation of thermal diffusivity (D), specific heat (C_p) and thermal conductivity (λ) with temperature for CVO and CVO-glass composite ceramic sintered at 740 °C and 650 °C respectively. C_p increases with increase in temperature as suggested by Debye model. D, remarkably a temperature dependent property, decreases almost linearly with temperature from room temperature to 200 °C.

The calculated values of the λ of CVO and CVO-glass composite ceramic from D, C_p and ρ is plotted in the Fig. 7a, b respectively. For CVO ceramic sintered at 740 °C, λ varies from 2.55 W/m K at room temperature to 2.44 W/m K at 200 °C, showing a more or less stable value with temperature. On the other hand, λ of CVO-glass composite decreases from 2.8 to 2.44 W/m K, with a small change in λ observed due to the addition of glass phase. Thermal

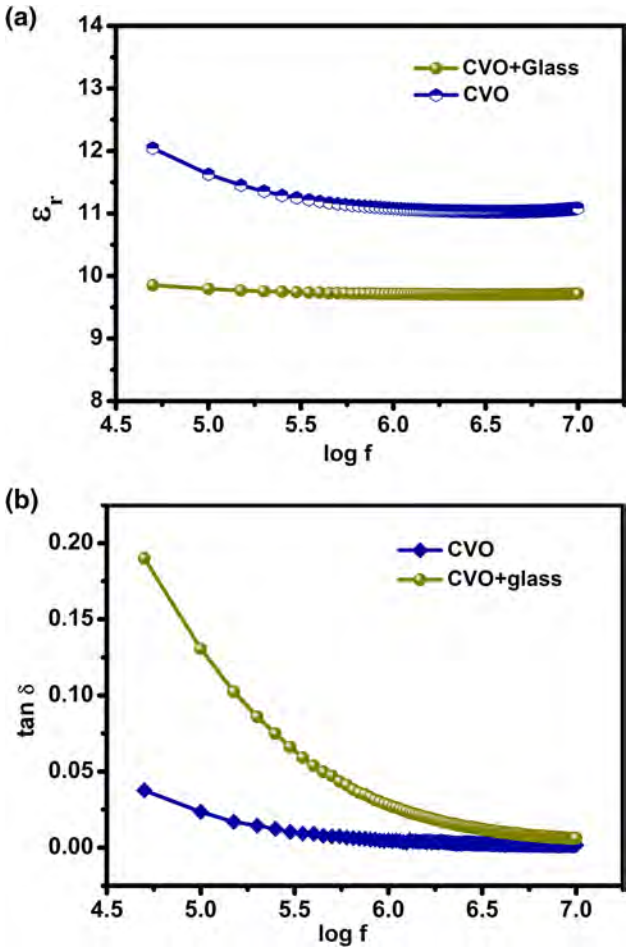

Fig. 6 Variation of **a** ε_r and **b** tanδ with frequency of CVO and CVO-glass composite ceramic sintered at 740 °C and 650 °C respectively

conductivity of ceramics is influenced by many parameters like porosity, shape and orientation of pores at temperature below 1200 °C. In CVO-glass composite ceramic, the small increase in λ compared to that of pure CVO is expected due to the reduction in porosity offered by the liquid phase sintering [49]. It is a known that materials with large atomic mass, loose chemical bonding and complex crystal structure with large number of atoms in a unit cell tend to possess relatively low thermal conductivity [50, 51]. Therefore, it can be assumed that CVO and its composite have low thermal conductivity. Figure 7a, b show the decrease in λ with

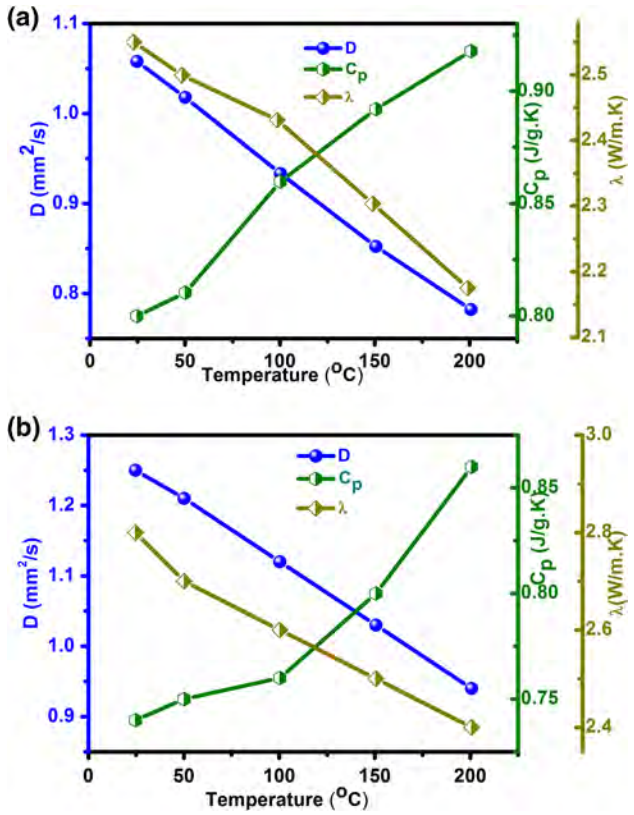

Fig. 7 Variation of D, C_p and λ with temperature of **a** CVO and **b** CVO-glass composite ceramic sintered at 740 °C and 650 °C respectively

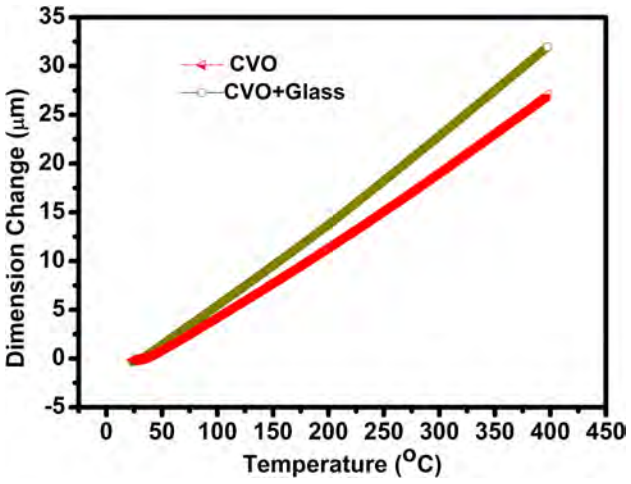

Fig. 8 Variation of linear dimension with temperature of CVO and CVO-glass composite ceramic sintered at 740 °C and 650 °C respectively

increasing temperature. These results are due to the proportionally reduced mean free path of phonon with increased phonon-phonon scattering. As a result, λ shows a falling off with increasing temperature [18, 52, 53].

3.7 Coefficient of thermal expansion

LTCC devices are designed in such a way that its linear coefficient of thermal expansion (CTE) should match with that of the associated device/components integrated onto it. For commercial substrates, CTE values are ~ 4 ppm/°C for connecting with semiconductors, 7–9 ppm/°C for alumina and 12–20 ppm/°C for printed circuit boards [45]. CTE mismatch between embedded semiconducting device and host ceramic substrate can cause mechanical failure in LTCC multilayer. High CTE ceramics can provide better reliability, as it can synchronize the expansion with that of high CTE metallization printed on it [54]. In the metavanadates, BaV_2O_6 is reported to have a CTE of 10 ppm/°C [12]. Figure 8 shows the change in dimension of the sintered samples as a function of temperature. The sintered ceramic of CVO and its glass composite have CTE values of 8.43 ppm/°C and 11.46 ppm/°C respectively. It is known that CTE of a material has close relationship with its bonding strength. Hence we can attribute the higher CTE of CVO and its glass composite to the week bonding between atoms [55].

We have developed ultra-low firing CaV_2O_6-glass composite ceramic green tape, which can be co-fired with Al metal at a temperature of 650 °C. Sintered laminates showed excellent thermal and dielectric properties. CVO-glass composite tape sintered at 650 °C possessed a dielectric constant of 10.6 and a low dielectric loss of 3.19×10^{-4} at 15 GHz, is highly promising for its commercial use as microelectronic substrate.

4 Conclusion

Ultra-low temperature co-fired ceramic substrates of CVO-glass composites were fabricated by tape casting technique. PPC/dimethyl carbonate based environmental friendly binder/solvent system was used for making high quality green tapes. The sintering temperature of CVO was lowered from 740 to 650 °C by adding 3 wt% of commercial glass for co-firing with aluminum metal. The added amorphous phase increased thermal conductivity from 2.55 to 2.8 W/m K as well as CTE from 8.43 to 11.46 ppm/°C compared to its pure form. The obtained thermal, mechanical and microwave dielectric properties of the CVO-glass composite substrate were highly satisfying for its application in microelectronic circuits as ULTCC substrates co-firable with aluminum electrode.

Acknowledgements The authors are grateful to the financial support from the brain pool program by KOFST (Grant No. 171S-2-1-1853,

2017) and ceramic strategic technology development program by KICET (Grant No. KPP17004-2, 2018).

References

1. Y. Li, Y. Xie, Ru Xie, D. Chen, H. Zhang, J. Alloys Compd. **737**, 144–151 (2018)
2. M.T. Sebastian, *Dielectric Materials for Wireless Communication* (Elsevier, Oxford, 2008), pp. 445–465
3. P. Abhilash, D. Thomas, K.P. Surendran, M.T. Sebastian, J. Am. Ceram. Soc. **96**, 1533–1537 (2013)
4. L.X. Pang, D. Zhou, W.B. Li, Z.X. Yue, J. Eur. Ceram. Soc. **37**, 3073–3077 (2017)
5. G. Subodh, R. Ratheesh, M.V. Jacob, M.T. Sebastian, J. Mater. Res. **23**, 1551–1556 (2008)
6. Z. Di, P. Li-Xia, Q. Ze-Ming, J. Biao-Bing, Y. Xi, Sci. Rep. **4**, 5980 (2014)
7. D. Zhou, C.A. Randall, H. Wang, L.-X. Pang, X. Yao, J. Am. Ceram. Soc. **93**, 1096–1100 (2010)
8. D. Zhou, D. Guo, W.-B. Li, L.-X. Pang, X. Yao, D.-W. Wang, I.M. Reaney, J. Mater. Chem. C **4**, 5357–5362 (2016)
9. E.K. Suresh, A.N. Unnimaya, A. Surjith, R. Ratheesh, Ceram. Int. **39**, 3635–3639 (2013)
10. H. Xiang, C. Li, Y. Tang, L. Fang, J. Eur. Ceram. Soc. **37**, 3959–3963 (2017)
11. E.K. Suresh, K. Prasad, N.S. Arun, R. Ratheesh, J. Electron. Mater. **45**, 2996–3002 (2016)
12. U.A. Neelakantan, S.E. Kalathil, R. Ratheesh, Eur. J. Inorg. Chem. **2**, 305–310 (2015)
13. G.-G. Yao, C.-J. Pei, J.G. Xu, P. Liu, J.-P. Zhou, H.-W. Zhang, J. Mater. Sci. Mater. Electron. **26**, 7719–7722 (2015)
14. S.E. Kalathil, U.A. Neelakantan, R. Ratheesh, J. Am. Ceram. Soc. **97**, 1530–1533 (2014)
15. A.C. Ali, E. Suvaci, H. Mandal, J. Eur. Ceram. Soc. **31**, 167–173 (2011)
16. M. Michálek, G. Blugan, T. Graule, J. Kuebler, Powder Technol. **274**, 276–283 (2015)
17. A. Kristoffersson, E. Carlström, J. Eur. Ceram. Soc. **17**, 289–297 (1997)
18. S. Arun, C.H. Kim, C.H. Lee, M.T. Sebastian, H.T. Kim, ACS Sustain. Chem. Eng. **6**, 6849–6855 (2018)
19. M. Ma, Y. Yang, D. Liao, P. Lyu, J. Zhang, J. Liang, L. Zhang, Appl. Organomet. Chem. **33**, e4708 (2018)
20. J. Honkamo, H. Jantunen, G. Subodh, M.T. Sebastian, P. Mohanan, Int. J. Appl. Ceram. Technol. **6**, 531–536 (2009)
21. H. Yu, K. Ju, J. Liu, Y. Li, J. Mater. Sci. Mater. Electron. **25**, 5114–5118 (2014)
22. T.I. Krasnenko, O.A. Zabara, L.V. Zolotukhina, A.A. Fotiev, J. Phys. Chem. Solids **60**, 645–650 (1999)
23. E.J. Baran, C.I. Cabello, A.G. Nordt, J. Raman Spectrosc. **18**, 405–407 (1987)
24. G. Perez, B. Frit, J.C. Bouloux, J. Galy, C. R. Acad. Sci., Ser. C. **270**, 952–953 (1970)
25. J.C. Bouloux, G. Perez, J. Galy, Bull. Soc. Fr. Mineral. Crystallogr. **95**, 130–133 (1972)
26. M. Schmidt, H. Münstedt, M. Svec, A. Roosen, T. Betz, F. Koppe, J. Am. Ceram. Soc. **85**, 314–320 (2004)
27. Y.T. Chou, Y.T. Ko, M.F. Yan, J. Am. Ceram. Soc. **70**, C-280–C-282 (1987)
28. A.I.Y. Tok, F.Y.C. Boey, Y.C. Lam, Mater. Sci. Eng. A. **280**, 282–288 (2000)
29. A. Feng, G. Wu, Y. Wang, C. Pan, J. Nanosci. Nanotechnol. **17**, 3859–3863 (2017)
30. M. Cai, J. Zhu, C. Yang, R. Gao, C. Shi, J. Zhao, Polymers **11**, 185 (2019)
31. J. Li, J. Ma, S. Chen, J. He, Y. Huang, Food Hydrocoll. **82**, 363–369 (2018)
32. H. Yan, W.R. Cannon, D.J. Shanefield, Ceram. Int. **24**, 433–439 (1998)
33. H. Yan, W.R. Cannon, D.J. Shanefield, J. Am. Ceram. Soc. **76**, 166–172 (1993)
34. G. Wu, Z. Jia, Y. Cheng, H. Zhang, X. Zhou, H. Wu, Appl. Surf. Sci. **464**, 472–478 (2018)
35. M. Ma, Y. Yang, W. Li, R. Feng, Z. Li, P. Lyu, Y. Ma, J. Mater. Sci. **54**, 323–334 (2019)
36. S. Masia, P.D. Calvert, W.E. Rhine, H.K. Bowen, J. Mater. Sci. **24**, 1907–1912 (1989)
37. S.M. Shapee, R. Alias, I. Azmi, Z. Ambak, Z.M. Yusoff, M.R. Saad, Key Eng. Mater. **421–422**, 485–489 (2009)
38. S.E. Fritz, T.W. Kelley, C.D. Frisbie, J. Phys. Chem. B. **109**, 10574–10577 (2005)
39. D. Monika, N. Suri, P.K. Khanna, Int. J. Res. Eng. Technol. **2**, 441–444 (2013)
40. Y. Gong, W. Deng, W. Zhang, C. Yatongchai, Y. Zou, R.C. Buchanan, Ceram. Int. **41**, 671–680 (2015)
41. G. Wu, H. Zhang, X. Luo, L. Yang, H. Lv, J. Colloid Interface Sci. **536**, 548–555 (2019)
42. T. Wu, Y. Pu, T. Zong, P. Gao, J. Alloys Compd. **584**, 461–465 (2014)
43. R.K. Bhuyan, T.S. Kumar, D. Pamu, Ferroelectrics **516**, 173–184 (2017)
44. T. Welker, S. Günschmann, N. Gutzeit, J. Müller, J. Ceram. Sci. Technol. **6**, 301–304 (2015)
45. M.T. Sebastian, H. Jantunen, Int. Mater. Rev. **53**, 57–90 (2008)
46. S. Arun, M.T. Sebastian, K.P. Surendran, Ceram. Int. **43**, 5509–5516 (2017)
47. M. Ma, Z. Liu, Y. Li, Y. Zeng, D. Yao, Ceram. Int. **39**, 4683–4687 (2013)
48. S. Wang, D. Zhang, X. Ouyang, Y. Wang, G. Liu, J. Alloys Compd. **667**, 23–28 (2016)
49. J. Kita, A. Engelbrecht, F. Schubert, A. Groß, F. Rettig, R. Moos, Sens. Actuators B **213**, 541–546 (2015)
50. R.C. Keller, R.O. Pohl, Phys. Rev. B **4**, 2029–2041 (1971)
51. R. Zhang, T.R. Wei, B.P. Zhang, K. Wang, D. Ichigozaki, J.F. Li, J. Alloys Compd. **646**, 298–302 (2015)
52. W.D. Kingery, J. Am. Ceram. Soc. **38**, 251–255 (1955)
53. S.B. Roshni, M.T. Sebastian, K.P. Surendran, Sci. Rep. **7**, 40839 (2017)
54. M. Eberstein, C. Glitzky, M. Gemeinert, T. Rabe, W.A. Schiller, C. Modes, Int. J. Appl. Ceram. Technol. **6**, 1–8 (2009)
55. L. Chen, P. Wu, P. Song, J. Feng, Ceram. Int. **44**, 16273–16281 (2018)